SEVENTH EUROPEAN ROTORCRAFT AND POWERED LIFT AIRCRAFT FORUM

Paper No.41

OPTIMUM PERFORMANCE AND WAKE GEOMETRY OF CO-AXIAL ROTOR IN HOVER

Tomoari Nagashima and Kenji Nakanishi
The National Defence Academy
Yokosuka, Japan

September 8-11, 1981
Garmisch-Partenkirchen
Federal Republic of Germany

Deutsche Gesellschaft für Luft- und Raumfahrt e.V.
Goethestr. 10, D-5000 Köln 51, F.R.G.

OPTIMUM PERFORMANCE AND WAKE GEOMETRY OF CO-AXIAL ROTOR IN HOVER

Tomoari Nagashima and Kenji Nakanishi
Department of Aeronautical Engineering,
The National Defense Academy
Yokosuka, Japan

ABSTRACT

Numerical studies to clear out the rotor-wake interference effects on the optimum performance and wake geometry of a co-axial rotor in hover are performed using the generalized momentum theory and the simplified free wake analysis. For applying the momentum concept to the performance predictions of the co-axial rotor system, each wake of rotors and flow fields around them are modeled so as to properly incorporate wake contractions, rotational velocities and nonlinear mutual interference effects. In case of the free wake analysis, it is approximated by a finite number of discrete circular vortices whose numbers and core radii are deduced from the sensitivity analysis. The numerical results clearly show that the performances and its wake geometries are largely dependent on the axial spacings and the pitch differences between rotors and there are unique combinations of them which could produce the optimum performance. It is also understood that the upwash effect of the contracted upper rotor wake on the lower rotor play a fundamental role to improve the hover performance with co-axial rotor arrangement.

1. INTRODUCTION

Although there are vast amount of experimental and analytical researches for an isolated single rotor, little have been conducted for a co-axial one and current knowledge about its aerodynamic characteristics are extremely limited. The key factors for the performance prediction of a co-axial rotor are the aerodynamic interferences and their precise estimation will become important for an advanced rotorcraft design.

It is well recognized, however, that even for a single rotor, the blade-wake interactions bring substantial effects on its performances and developments of suitable methods to be consistent with wake deformations are urgently desired. Most straight forward procedures for these seem to be computer orientated numerical procedures which can be succeeded to clarify the detail relationship between wake geometry and hover performance in some degrees[1].

As for performances of a co-axial rotor in hover, W. Z. Stepniewski and W. Johnson have given brief descriptions in ref. 2 and ref. 3. Several theoretical developments for a co-axial rotor in U.S.S.R. were found in ref. 4. The concept of the variable geometry rotor (V.G.R.) was proposed by A. J. Landgrabe et al[5] recently and possibilities to improve the hover performance were pointed out by reorientation of tip vortices trajectories with the proper co-axial rotor arrangement. This is just a experimental study but to the best of the author's knowledge, it is a first attempt for a performance optimization with a dual rotor system. A comparative study on the accuracies of several prediction methods with experimental results was made by M. J. Andrew for the hover performance of the remotely piloted co-axial rotor[6].

Apart from these, experimental studies on the hover performance of a co-axial, contra-rotating rotor with variable axial spacing have been executed at our laboratory and the basic data governing its optimum performance were successively grapsed within experimental accuracies[7]. Flow visualizations were also conducted to clarify the flow fields around a co-axial rotor under various operating conditions[8].

The purpose of this paper is to develop analytical methods for the performance prediction of a co-axial rotor in hover and establish its optimum performance in relation to the wake geometry. Based on the flow visualization results on the model co-axial rotor, the flow fields in near and far wakes of each rotor are modeled to properly incorporate mutual interactions. The generalized momentum theory which take into account of wake contraction and rotational velocity effects is applied to the mathematical model and the thrust, the induced torque and the power of a co-axial rotor are expressed as the functionals of the far wake axial velocities. The optimum performance is formulated as a calculus of variation problem to determine the specific thrust sharing ratio which could minimize the total induced power for the given thrust with the axial spacing as a parameter. It is understood that the optimal conditions are always consistent with the torque balance at any axial spacing whereas the thrust sharing ratio for optimum performance is largely dependent on the axial spacing and it is almost equal to the contraction ratio of the upper rotor wake at the lower rotor disc. These fundamental features to be explored by the momentum analysis are closely related to the flow field structures of the outer part of the lower rotor where the contributions of the upwash effects of the contracted upper rotor wake are predominated.

For more rigorous treatments of these rotor-wake interactions on the hover performance of a co-axial rotor, the simplified free wake analysis is also carried out. In this case, for simplicity of numerical procedures, each wake of b-bladed rotor is approximated by a finite number of discrete circular vortices whose numbers to be involved and their vortex core radii are deduced from the sensitivity analysis. As already mentioned in the application of the free wake analysis to a single rotor, the convergence of the wake geometry is not always ensured, the iterations are truncated when the spacial arrangements of the first four circular vortices of each rotor change by less than the convergent criteria between two successive iterations. It is shown that the wake geometries of a co-axial rotor in hover are remarkably varied with the combinations of the thrust sharing ratios and the axial spacings between rotors and the most important cues to define the optimum performance are found in behaviours of the near wake geometry of the lower rotor. These unique properties to govern the optimum hover performance of a co-axial rotor in hover are well consistent with the results of model rotor tests and the usefulness and accuracies of the proposed wake models and numerical approaches are ascertained.

2. FORMULATION OF OPTIMUM HOVER PERFORMANCE BY GENERALIZED MOMENTUM THEORY

2.1 MATHEMATICAL MODEL AND BASIC RELATIONS

Let us consider a co-axial, contra-rotating rotor hovering in incompressive and inviscid fluid. The flow is assumed to be steady and axisymmetric. Each rotor of them which are separated with the axial spacing, D is replaced by an actuator disc and flow fields around them are modeled so as to properly incorporate wake-rotor interactions. Wake contractions and

rotational velocities in each rotor wake are also taken into account. The mathematical model to be used is shown in Fig. 1. Significant features of this model are that the slipstream of each rotor is clearly defined and the flow fields around the lower rotor are divided into two distinct regions, one is the inner region where the air mass will be affected by the downwash velocity of the upper rotor and the other is the outer one where it will be subjected to the upwash velocity.

Let r, dS, W and ωr be the radius of any annular element, its elemental area, axial and rotational velocities of fluid, respectively and distinguish these quantities at different locations by number in the subscript as defined in Fig. 1. Then the basic relations to be used in this analysis are read as follows,

(a) Continuities of mass flow:

$$W_1 dS_1 = W_2 dS_2 = W_3 dS_3 \tag{1}$$

$$W_{20} dS_{20} = W_{30} dS_{30} \tag{2}$$

(b) Conservations of angular momentum:

$$\omega_1' r_1^2 = \omega_2 r_2^2 = K_{r_1},\ \omega_2' r_2^2 = K_{r_2}$$

$$\omega_3 r_3^2 = (\omega_2 - \omega_2') r_2^2 = K_{r_1} - K_{r_2} = K_{r_3} \tag{3}$$

$$\omega_{30} r_{30}^2 = \omega_{20}' r_{20}^2 = K_{r_{20}} \tag{4}$$

(c) Bernoulli's equations:

$$(P_1' - P_1) + (P_2' - P_2) + (P_0 - P_3)$$

$$= \frac{1}{2}\rho W_3^2 + \frac{1}{2}\rho(\omega_2 - \omega_1')K_{r_1} + \frac{1}{2}\rho[\omega_3 - (\omega_2 - \omega_2')]K_{r_3} \tag{5}$$

$$(P_{20}' - P_{20}) + (P_0 - P_3) = \frac{1}{2}\rho W_{30}^2 + \frac{1}{2}\rho(\omega_{30} - \omega_{20}')K_{r_{20}} \tag{6}$$

where K_{r_i} (i = 1, 2, 3) and $K_{r_{20}}$ are the circulations of fluid in each region and P, ρ are the pressure and density of fluid, respectively. Quantities with prime indicate to take their values at the lower side of each rotor.

As there is no flow entering at far ahead of rotors and no contraction of slipstream at far wake of each rotor, the axial momentum crossing the control surface which is selected as a plane surface perpendicular to the rotor axis at the far wake of each rotor give the following force relations,

$$\int_{s_1} dT_u + \int_{s_2} dT_\ell^{in} = \int_{s_3} \rho W_3^2 dS_3 - \int_{s_3} (P_0 - P_3) dS_3 \tag{7}$$

$$\int_{s_{20}} dT_\ell^{out} = \int_{s_{30}} \rho W_{30}^2 dS_{30} - \int_{s_{30}} (P_0 - P_{30}) dS_{30} \tag{8}$$

or in differential forms,

$$dT_u + dT_\ell^{in} = \rho W_3^2 dS_3 - (P_0 - P_3)dS_3 \tag{7}'$$

$$dT_\ell^{out} = \rho W_{30}^2 dS_{30} - (P_0 - P_{30})dS_{30} \tag{8}'$$

where dT_u is the elemental thrust generated by an annular element at the upper rotor and dT_ℓ^{in}, dT_ℓ^{out} are those generated by annular elements at the inner and outer portions of the lower rotor, respectively. Then the total thrust of the co-axial rotor becomes

$$T = T_u + T_\ell^{in} + T_\ell^{out} = \int_{S_3} \rho W_3^2 dS_3 + \int_{S_{30}} \rho W_{30}^2 dS_{30}$$
$$- \int_{S_3} (P_0 - P_3)dS_3 - \int_{S_{30}} (P_0 - P_{30})dS_{30} \tag{9}$$

Alternate equations for (7)', (8)' are given by expressing these thrusts with the pressure jump at each rotor,

$$(P_1' - P_1)dS_1 + (P_2' - P_2)dS_2 + (P_0 - P_3)dS_3 = \rho W_3^2 dS_3 \tag{10}$$

$$(P_{20}' - P_{20})dS_{20} + (P_0 - P_{30})dS_{30} = \rho W_{30}^2 dS_{30} \tag{11}$$

where the pressure jumps can be obtained by applying Bernoulli's equation to the flows relative to each rotor blades. As each rotor is rotating in opposite directions with the same revolutional speed, Ω and there is no discontinuity in axial and radial velocities, the pressure jumps are given by

$$P_1' - P_1 = \rho(\Omega - \frac{\omega_1'}{2})K_{r_1} \tag{12}$$

$$P_2' - P_2 = \rho[\Omega - (\frac{\omega_2'}{2} - \omega_2)]K_{r_2} \tag{13}$$

$$P_{20}' - P_{20} = \rho(\Omega - \frac{\omega_{20}'}{2})K_{r_{20}} \tag{14}$$

According to eqs. (12), (13) and (14), we can express the total thrust given in eq. (9) in terms of the circulations by

$$T = \int_{S_1} \rho(\Omega - \frac{\omega_1'}{2})K_{r_1} dS_1 + \int_{S_2} \rho[\Omega - (\frac{\omega_2'}{2} - \omega_2)]K_{r_2} dS_2$$
$$+ \int_{S_{20}} \rho(\Omega - \frac{\omega_{20}'}{2})K_{r_{20}} dS_{20} \tag{15}$$

and define the thrust sharing ratio between the upper and lower rotor as

$$\tau = \frac{T_\ell^{in} + T_\ell^{out}}{T_u} = \frac{\int_{S_2} \rho[\Omega - (\frac{\omega_2'}{2} - \omega_2)]K_{r_2} dS_2 + \int_{S_{20}} \rho(\Omega - \frac{\omega_{20}'}{2})K_{r_{20}} dS_{20}}{\int_{S_1} \rho(\Omega - \frac{\omega_1'}{2})K_{r_1} dS_1} \tag{16}$$

Besides from eqs. (5) and (6), the pressure difference in the far wakes are also written as

$$P_0 - P_3 = \frac{1}{2}\rho W_3^2 - \rho(\Omega - \frac{\omega_2}{2})K_{r_1} - \rho[\Omega - (\frac{\omega_2'}{2} - \omega_2)]K_{r_2}$$

$$+ \frac{1}{2}\rho[\omega_3 - (\omega_2 - \omega_2')]K_{r_3} \tag{17}$$

$$P_0 - P_{30} = \frac{1}{2}\rho W_{30}^2 - \rho(\Omega - \frac{1}{2}\omega_{30})K_{r_{20}} \tag{18}$$

Substituting eqs. (17) and (18) into eqs. (10), (11) with applying eqs. (1) and (2), yield

$$\frac{W_3}{2} = [\frac{\Omega - \frac{1}{2}\omega_1'}{W_1} - \frac{\Omega - \frac{1}{2}\omega_2}{W_3}]K_{r_1} + [\frac{\Omega - (\frac{1}{2}\omega_2' - \omega_2)}{W_2} - \frac{\Omega - (\frac{1}{2}\omega_2' - \omega_2)}{W_3}]K_{r_2}$$

$$+ [\frac{\frac{1}{2}\omega_3}{W_3} - \frac{\frac{1}{2}(\omega_2 - \omega_2')}{W_3}]K_{r_3} \tag{19}$$

$$\frac{W_{30}}{2} = [\frac{\Omega - \frac{1}{2}\omega_{20}'}{W_{20}} - \frac{\Omega - \frac{1}{2}\omega_{30}}{W_{30}}]K_{r_{20}} \tag{20}$$

Eqs. (19) and (20) constitute the general equations which describe the relations between the far wake axial velocities and rotational velocities for co-axial rotor in hover. It is easily shown that these equations are reduced to the H. Glauert's result[9] for a single propeller if we put $K_{r_2} = K_{r_3} = K_{r_{20}} = 0$ into eqs. (19) and (20).

The torque and induced power equations are also obtained in similar way by considering the angular momentum change and work done at each rotor in unit time and they are summarized as follows.

$$dQ_u = (\rho W_1 dS_1)K_{r_1} \tag{21}$$

$$dQ_\ell^{in} = (\rho W_2 dS_2)K_{r_2} = dQ_u K_{r_2}/K_{r_1} \tag{22}$$

$$dQ_\ell^{out} = (\rho W_{20} dS_{20})K_{r_{20}} \tag{23}$$

$$Q = \int_{S_1}\rho W_1 K_{r_1} dS_1 + \int_{S_2}\rho W_2 K_{r_2} dS_2 + \int_{S_{20}}\rho W_{20} K_{r_{20}} dS_{20} \tag{24}$$

$$d\bar{P}_u = W_1 dT_u + \frac{1}{2}\omega_1' dQ_u \tag{25}$$

$$d\bar{P}_\ell^{in} = W_2 dT_\ell^{in} + (\frac{1}{2}\omega_2' - \omega_2)dQ_\ell^{in} \tag{26}$$

$$d\bar{P}_\ell^{out} = W_{20} dT_\ell^{out} + \frac{1}{2}\omega_{20}' dQ_\ell^{out} \tag{27}$$

$$\bar{P} = \int_{s_1} W_1 dT_u + \int_{s_2} W_2 dT_\ell^{in} + \int_{s_{20}} W_{20} dT_\ell^{out} + \frac{1}{2}\int_{s_1} \omega_1' dQ_u$$

$$+ \int_{s_2} (\frac{\omega_2'}{2} - \omega_2) dQ_\ell^{in} + \frac{1}{2}\int_{s_{20}} \omega_{20}' dQ_\ell^{out} \qquad (28)$$

where Q, $\bar{P}$ are the total torque and the induced power, dQ_u, $d\bar{P}_u$ are the elemental torque and the elemental induced power of the upper rotor, dQ_ℓ^{in}, $d\bar{P}_\ell^{in}$ are those at the inner part of the lower rotor and dQ_ℓ^{out}, $d\bar{P}_\ell^{out}$ are those at the outer part of the lower rotor, respectively. The power sharing ratio between rotors, ν is defined as

$$\nu = \frac{\bar{P}_\ell^{in} + \bar{P}_\ell^{out}}{\bar{P}_u}$$

$$= \frac{\int_{s_2} W_2 dT_\ell^{in} + \int_{s_{20}} W_{20} dT_\ell^{out} + \int_{s_2} (\frac{\omega_2'}{2} - \omega_2) dQ_\ell^{in} + \frac{1}{2}\int_{s_{20}} \omega_{20}' dQ_\ell^{out}}{\int_{s_1} W_1 dT_u + \frac{1}{2}\int_{s_1} \omega_1' dQ_u} \qquad (29)$$

2.2 OPTIMAL CONDITIONS AND OPTIMUM PERFORMANCE

Owing to the rotational motions of fluids at the far wakes, the radial pressure gradients in these regions must be balanced with the centrifugal forces, namely

$$\frac{dP_3}{dr_3} = \rho r_3 W_3^2 \quad , \quad \frac{dP_{30}}{dr_{30}} = \rho r_{30} W_{30}^2 \qquad (30)$$

The pressure gradients can be derived by differentiating eqs. (17) and (18) with r_3 and r_{30}, respectively. Combining these results with eq. (30) and assuming that the axial velocities at the far wakes are constant across their regions, that is, $dW_3/dr_3 = 0$, $dW_{30}/dr_{30} = 0$, then we obtain

$$\frac{1}{2}\frac{d}{dr_3}(W_3)^2 = (\Omega - \frac{\omega_2}{2})\frac{d}{dr_3}(K_{r_1}) + [\Omega - (\frac{\omega_2'}{2} - \omega_2)]\frac{d}{dr_3}(K_{r_2})$$

$$- \frac{1}{2}[\omega_3 - (\omega_2 - \omega_2')]\frac{d}{dr_3}(K_{r_3}) - \frac{1}{2}[K_{r_1}\frac{d\omega_2'}{dr_3} - K_{r_2}\frac{d\omega_2}{dr_3}]$$

$$- \frac{1}{2}[\frac{d}{dr_3}(\omega_3 K_{r_3}) - K_{r_3}\frac{d\omega_3}{dr_3}] = 0 \qquad (31)$$

$$\frac{1}{2}\frac{d}{dr_{30}}(W_{30}^2) = (\Omega - \omega_{30})\frac{d}{dr_{30}}(K_{r_{30}}) = 0 \qquad (32)$$

By inspecting eqs. (31) and (32), the optimal conditions with which the ideal distributions of the circulations and the angular velocities at the wakes should be satisfied are led to

$$K_{r_1} = K_{r_2} = K_1 = \text{Const, and } K_{r_3} = 0$$

$$K_{r_{20}} = K_{r_{30}} = K_2 = \text{Const} \qquad (33)$$

$$\omega_2 = \omega_2' \quad , \quad \omega_3 = 0$$

At the same time from eqs. (1), (2) and (3), (4), yield

$$\frac{W_2}{W_1} = \frac{\omega_2}{\omega_1} = \frac{R^2}{R_2^2} \quad , \quad \frac{W_{30}}{W_{20}} = \frac{\omega_{30}}{\omega_{20}'} = \frac{R^2}{R_{30}^2} \tag{34}$$

where R is the radius of each rotor, R_2 is the radius of cross section of the contracted upper rotor wake at the lower rotor and R_{30} is the radius of cross section of the contracted lower rotor at the far wake, respectively.

Under the optimal conditions given in eqs. (33), (34), P_3 becomes equal to P_0, then K_1 is given by $K_1 = W_3^2/4\Omega$ and further eqs. (19) and (20) are reduced to more simple relations,

$$\frac{4}{W_3} = \frac{1}{W_1} + \frac{1}{W_2} \tag{35}$$

$$\frac{W_{30}}{2} = \left(\frac{1}{W_{20}} - \frac{1}{W_{30}}\right)\Omega K_2 \tag{36}$$

It is interesting to note that under the optimal conditions, the axial velocities at the inner wake region can be determined independent of the rotational ones and this is originated from the contra-rotation effect of co-axial rotor.

Applying the optimal conditions to eqs. (15), (28) and other related equations and nondimensionalizing them with $2\rho(\Omega R)^2\pi R^2$ and $2\rho(\Omega R)^3\pi R^2$, respectively, we obtain, after lengthly but simple calculations, the following equations for the total thrust and the total induced power of a co-axial rotor in hover at the optimal conditions.

$$C_T = \frac{1}{8}\lambda_3^2(1 + \tau) + \varepsilon_1 \tag{37}$$

$$C_P = \left(\frac{\lambda_3}{2}\right)^2\left[\lambda_1 + \frac{\lambda_{20}}{2}(\tau - \alpha)\right] + \varepsilon_2 \tag{38}$$

where C_T, C_P are the nondimensional thrust and the power coefficients, α is the contraction ratio of the upper rotor wake at the lower rotor and λ_1, λ_3, λ_{20} are the axial inflow ratio at each region of wakes which are respectively, defined by

$$C_T = \frac{T}{2\rho\pi R^2(\Omega R)^2} \quad , \quad C_P = \frac{\bar{P}}{2\rho\pi R^2(\Omega R)^3}$$
$$\alpha = \frac{\pi R_2^2}{\pi R^2} \quad , \quad \lambda_1 = \frac{W_1}{\Omega R} \quad , \quad \lambda_3 = \frac{W_3}{\Omega R} \quad , \quad \lambda_{20} = \frac{W_{20}}{\Omega R} \tag{39}$$

ε_1 and ε_2 in eqs. (37) and (38) indicate the thrust and the power losses due to the rotational motions of fluids at the outer part of the lower rotor wake and are higher than 3rd order term in λ_3. In this analysis, these are reasonably neglected being small quantities compared with the first terms in their equations.

Now, we intend to introduce the mutual interference effects into the nondimensional axial velocities at each wake region as follows.

$$\lambda_1 = \lambda_u + k'\lambda_\ell \tag{40}$$

$$\lambda_2 = \lambda_\ell + k\lambda_u, \text{ and } \lambda_{20} = \lambda_\ell - k''\lambda_u \tag{41}$$

where λ_u, λ_ℓ are defined by

$$\lambda_u = \sqrt{\frac{C_T}{1+\tau}} \quad , \quad \lambda_\ell = \sqrt{\frac{\tau}{1+\tau} C_T} \tag{42}$$

and interaction factors k, k', k" are given as the functions of the axial spacing, D, by

$$k = 1 + \frac{D/R}{\sqrt{1+D^2/R^2}} \quad , \quad k' = 2 - k \quad , \quad k'' = \frac{1}{\sqrt{k}} \tag{43}$$

Though in eqs. (40) and (41), the mutual interactions between rotors are assumed to be linear, but for moderate axial spacing, upwash effect at the outer part of the lower rotor is reasonably accounted for. Substituting eqs. (40), (41) into eqs. (37), (38) with using eqs. (35), (36), the total thrust and the power of a co-axial rotor can be expressed as functionals of the thrust sharing ratio, τ and its optimum performances are established to determine the specific thrust sharing ratio which could minimize the total induced power for the given thrust with the axial spacing as a parameter.

Typical computed results for the optimum performance of a co-axial rotor are shown in Fig. 2 where experimental results with the model co-axial rotor test are also plotted for comparisons. θ_u and θ_ℓ in Fig. 2 indicate the collective pitch angles of the upper and lower rotor blades of the model co-axial rotor, respectively. The coincidence between the computed and experimental results is quite well for any axial spacing in practical uses. The essential features of the optimum performance and its wake geometry to be explored by the generalized momentum analysis are summarized as follows.

(1) The optimal conditions are always consistent with the torque balance between rotors at any axial spacing whereas the thrust sharing ratio for the optimum performance is largely dependent on the axial spacing.

(2) The optimum thrust sharing ratio for the given axial spacing is almost equal to the contraction ratio of the upper rotor wake at the lower rotor.

(3) The optimum performance could be realized if and only if the axial velocities become zero or the ideal auto-rotation state can be built up at the outer part of the lower rotor.

3. THE OPTIMUM WAKE GEOMETRY OF CO-AXIAL ROTOR IN HOVER BY SIMPLIFIED FREE WAKE ANALYSIS

3.1 SIMPLIFIED FREE WAKE ANALYSIS

As already mentioned in the generalized momentum analysis, the optimum performance of a co-axial rotor in hover could be realized only at the

specified thrust sharing ratio between rotors at which the optimum wake geometry would be formulated for each rotor. In this section, for more rigorous treatments of the mutual interaction effects for the hover performances of the co-axial rotor, the nonlinear vortex theory using the free wake analysis is developed.

For simplicity of numerical procedures, the following assumptions are made.

(1) Each rotor being separated vertically with the axial spacing, D, has a same geometrical properties and counter rotate with the same rotational speed, Ω.

(2) Each rotor blade is represented by a lifting line with the uniform circulation distribution.

(3) Each wake of rotors is consist of a finite number of discrete circular vortices, N and the strength of the vorticity along any circular vortex is equal to that of the bound circulation.

(4) The fluid is to be incompressive, inviscid and the viscous diffusion effects of the vortex is neglected.

(5) Each circular vortex have a finite vortex core radius and its self induced velocity is determined by the Lamb's formula.

According to these assumptions, the initial wake geometry of each rotor will be arranged with a finite number of equi-radius circular vortices at regular intervals

$$d_u = \frac{2\pi W_1}{B\Omega} \quad , \quad d_\ell = \frac{2\pi W_{20}}{B\Omega} \tag{44}$$

where d_u, d_ℓ are the elemental axial spacings between two successive vortices of the upper and the lower rotor wakes, B is the blade number of each rotor and W_1, W_{20} are the axial induced velocities at the upper and the lower rotor defined in the proceeding momentum analysis, respectively. Hence the coordinates of the jth circular vortex of each rotor are given by

$$\begin{aligned} r_j^u &= R \quad , \quad Z_j^u = jd_u \\ r_j^\ell &= R \quad , \quad Z_j^\ell = D + jd_\ell \qquad (j = 1, 2, \ldots, N) \end{aligned} \tag{45}$$

in the cylindrical coordinate (r, θ, Z) with the origin at the center of the upper rotor and the Z axis coinciding with the rotor axis and pointing downward.

Although the initial wake geometries are very simple ones, they are in general not always satisfy the force equilibrium conditions and vortices will change their positions subject to the mutual interaction effects between them. Then let $\vec{S}_i(t)$ be the position vector of a particle on the ith circular vortex filament at time, t, the new position vector of the particle Δt_ψ later is given by

$$\vec{S}_i(t + \Delta t_\psi) = \vec{S}_i(t) + \vec{U}_i(t)\Delta t_\psi \qquad (i = 1, 2, \ldots, 2N) \qquad (46)$$

where Δt_ψ is a time required the blade to rotate a incremental azimuth angle, $\Delta\psi$ and $\vec{U}_i(t)$ is the total velocity of the particle which is considered to remain constant during a small time interval, Δt_ψ. The total velocity $\vec{U}_i$, can be given by

$$\vec{U}_i = \sum_{k=1,\neq i}^{2N} \vec{v}_{k,i}^{ind} + \vec{v}_i^{self} = \vec{V}_i^{ind} + \vec{v}_i^{self} \qquad (i = 1, 2, \ldots, 2N) \qquad (47)$$

where $\vec{v}_{k,i}^{ind}$ is the mutual induced velocity at the ith circular vortex filament due to the kth circular vortex, $\vec{V}_i^{ind}$ is the total induced velocity due to all but the ith circular vortices and $\vec{v}_i^{self}$ is the self induced velocity of the ith circular vortex.

The mutual induced velocities, $\vec{v}_{k,i}^{ind}$, $\vec{V}_i^{ind}$, are obtained by applying the Biot-Savart's law to the vortex system shown in Fig. 3. Because of axisymmetric nature of the vortex system, it is obvious that there is no circumferential flow component and $\vec{V}_i^{ind}$ can be expressed in the closed form as

$${}_rV_i^{ind} = \sum_{k=1,\neq i}^{2N} \left(\frac{\gamma_k}{4\pi}\right)\left(\frac{Z_{ik}}{\delta_{ik} r_i}\right)\left[\frac{2 - \sigma_{ik}^2}{1 - \sigma_{ik}^2} E(\sigma_{ik}) - 2K(\sigma_{ik})\right] \qquad (48)$$

$${}_ZV_i^{ind} = \sum_{k=1,\neq i}^{2N} \left(\frac{\gamma_k}{4\pi}\right)\frac{1}{\delta_{ik}}\left[\frac{r_{ik}/r_i - 2}{1 - \sigma_{ik}^2} E(\sigma_{ik}) + 2K(\sigma_{ik})\right] \qquad (49)$$

with

$$\begin{aligned} r_{ik} &= R_i + r_k \quad , \quad Z_{ik} = Z_i - Z_k \\ \delta_{ik}^2 &= r_{ik}^2 + Z_{ik}^2 \quad , \quad \sigma_{ik}^2 = \frac{4 r_i r_k}{\delta_{ik}^2} \\ K(\sigma) &= \int_0^{\frac{\pi}{2}} \frac{d\alpha}{\sqrt{1 - \sigma^2 \mathrm{Sin}^2\alpha}} \quad , \quad E(\sigma) = \int_0^{\frac{\pi}{2}} \sqrt{1 - \sigma^2 \mathrm{Sin}^2\alpha}\, d\alpha \end{aligned} \qquad (50)$$

$$(i = 1, 2, \ldots, 2N)$$

where ${}_rV_i^{ind}$, ${}_ZV_i^{ind}$ are the radial and the axial components of the induced velocity at the ith circular vortex, γ_k is the vorticity of the kth circular vortex, (r_i, Z_i) and (r_k, Z_k) are the radial and the axial coordinates of the ith and the kth circular vortices, respectively. $E(\sigma)$ and $K(\sigma)$ are the complete elliptic integrals of the lst and the 2nd kinds.

While $\vec{v}_i^{self}$, the second term in eq. (47), is represented by the Lamb's formula[10] for the self induced velocity of the circular vortex with the finite core radius, ε and each component of them are given by

$$\begin{aligned} {}_rv_i^{self} &= 0 \quad , \quad {}_\theta v_i^{self} = 0 \\ {}_Zv_i^{self} &= \frac{\gamma_i}{4\pi r_i}\left[\log\left(\frac{8 r_i}{\varepsilon}\right) - \frac{1}{4}\right] \end{aligned} \qquad (51)$$

$$(i = 1, 2, \ldots, 2N)$$

where ${}_r v_i^{self}$, ${}_\theta v_i^{self}$ and ${}_z v_i^{self}$ are the radial, the tangential and the axial components of the self induced velocity of the ith circular vortex.

From assumption (3), the vorticity of the ith circular vortex, γ_i, is easily given by

$$\gamma_i = \frac{2C_{T_u}}{B}\Omega R\pi R \qquad \text{or} \qquad = \frac{2C_{T_\ell}}{B}\Omega R\pi R \quad (i = 1, 2, \ldots, 2N) \tag{52}$$

depending on the situation whether the ith circular vortex to be considered will attribute to one of the upper or the lower rotor wake. C_{T_u} and C_{T_ℓ} in (52) are nondimensional thrust coefficient of the upper and the lower rotor, defined as $C_{T_u} = T_u/\rho\pi R^2(\Omega R)^2$ and $C_{T_\ell} = T_\ell/\rho\pi R^2(\Omega R)^2$, respectively.

When the time elapsed will become equal to that of one revolution of the blade after n times iterations, that is, $n\Delta t_\psi = \Delta t_{2\pi}$, then the new circular vortex is fed into each rotor wake and the oldest Nth vortex is removed from each wake simultaneously, conserving the total number of vortices to be involved in the wakes as 2N. During the iterations, if the spacial coordinate of the kth vortex come close to that of the ith one, singulalities may be encountered in numerical evaluation of $\vec{v}_{i,k}^{ind}$. To avoid these difficulties, when the relative distance between the ith and the kth circular vortices filaments become less than their vortex core radii, ε, each component of the mutual induced velocity $\vec{v}_{i,k}^{ind}$ is simply replaced by those of the self induced velocity, $\vec{v}_k^{self}$.

From mathematical point of view, it is desired that the numerical procedures are successively repeated until a converged wake geometry for each rotor could be resulted. However, as already indicated in several researches for a single rotor[11),12)], the convergence of the wake geometries of each rotor in the far wake regions are not always ensured and the necessity to take account of the viscous diffusions of the vortices would be desired. In this analysis, the iterations are truncated when the spacial arrangement of the first four circular vortices of each rotor changes by less than the convergent criteria between two successive iterations.

3.2 INDUCED VELOCITY AND AERODYNAMIC FORCES ACTING ON EACH ROTOR

In previous discussion, the wake deformations of a co-axial rotor in hover are determined with the assumption that the aerodynamic forces or the bound circulation of each rotor blades will be given in advance. Then the final step to complete the iteration procedures is to define the induced velocity distribution and the aerodynamic forces acting on each rotor which should be consistent with the each deformed wake geometry.

The induced velocity distributions along each rotor blade are also obtained by applying the same procedures as those of the determination of the mutual induced velocities between circular vortices and the axial component of them can be expressed in the closed form by

$$W_u(r) = \sum_{i=1}^{2N} \left(\frac{\gamma_i}{4\pi}\right)\frac{1}{\delta_u}\left[\frac{r_u/r_i - 2}{1 - \sigma_u^2}E(\sigma_u) + 2K(\sigma_u)\right]$$

$$W_\ell(r) = \sum_{i=1}^{2N} \left(\frac{\gamma_i}{4\pi}\right)\frac{1}{\delta_\ell}\left[\frac{r_\ell/r_i - 2}{1 - \sigma_\ell^2}E(\sigma_\ell) + 2K(\sigma_\ell)\right] \tag{53}$$

where $W_u(r)$, $W_\ell(r)$ are the axial induced velocities at any radial position, r on the upper and the lower rotor blade, r_i and Z_i are the radial and the axial coordinates of the ith circular vortex, respectively. $E(\sigma)$ and $K(\sigma)$ are, of course, the complete elliptic integrals of the 1st and 2nd kinds defined in (50) and r_u, r_ℓ, δ_u, δ_ℓ, σ_u, σ_ℓ are defined as follows,

$$
\begin{aligned}
& r_u = r + r_i \quad , \quad r_\ell = r + r_i \\
& \delta_u^2 = r_u^2 + (Z_i - r\beta_u)^2, \ \delta_\ell^2 = r_\ell^2 + (Z_i - D + r\beta_\ell)^2 \\
& \sigma_u^2 = \frac{4rr_i}{\delta_u^2} \quad , \quad \sigma_\ell^2 = \frac{4rr_i}{\delta_\ell^2}
\end{aligned}
\tag{54}
$$

where β_u, β_ℓ are the coning angles of the upper and the lower rotor blades.

With the assistance of eq. (53), the steady aerodynamic forces acting on each rotor blades can be determined by various methods. In practice, the performance calculations are made by the simple blade element theory using constant lift curve slop, a, and profile drag coefficient, δ_0, which yields the thrust and torque relations for each rotor as follows,

$$
\begin{aligned}
T_u &= \frac{B}{2}\rho ac\Omega^2 \int_0^R [\theta_u - \frac{W_u(r)}{\Omega r}] r^2 dr \\
T_\ell &= \frac{B}{2}\rho ac\Omega^2 \int_0^R [\theta_\ell - \frac{W_\ell(r)}{\Omega r}] r^2 dr
\end{aligned}
\tag{55}
$$

$$
\begin{aligned}
Q_u &= \frac{B}{8}\rho\delta_0 c\Omega^2 R^4 + \frac{B}{2}\rho ac\Omega^2 \int_0^R [\theta_u - \frac{W_u(r)}{\Omega r}] r^3 dr \\
Q_\ell &= \frac{B}{8}\rho\delta_0 c\Omega^2 R^4 + \frac{B}{2}\rho ac\Omega^2 \int_0^R [\theta_\ell - \frac{W_\ell(r)}{\Omega r}] r^3 dr
\end{aligned}
\tag{56}
$$

where $W_u(r)$, $W_\ell(r)$ are the axial induced velocities defined in eq. (53), c is the blade chord length, θ_u and θ_ℓ are the pitch angles of the upper and lower rotor blades, respectively.

3.3 NUMERICAL RESULTS AND DISCUSSIONS

Processing to the systematic applications of the above described numerical procedures for computations of the wake geometries of the co-axial rotor in hover, the sensitivity analysis for the azimuth increment, $\Delta\psi$, the number of the circular vortices to be involved in the wakes, N and the vortex core radius, ε, are conducted. The prediction accuracies of this method are considered in general to be improved by decreasing the azimuth increment, $\Delta\psi$, increasing the number of the vortex, N and proper selection of the vortex core size, ε, however, the results of the sensitivity analysis show that the prediction accuracies can be guaranteed with adoptation of $\Delta\psi = 20°$, N = 8 for each rotor and $\varepsilon = 0.05R$ for practical uses.

Sample performance calculations are also made using eqs. (55), (56) with $a \approx 5.73$ and $\delta_0 = 0.015$ for the model co-axial rotor which has two uniform blades for each rotor with a radius of 1.0m, a chord length of 0.08m and a airfoil cross section of NACA 0012. The blades are hinged at each rotor hub with a hinge-offset of 20% radius and each rotor is counter rotated with a revolutional speed of 500 R.P.M.

The typical computed results of the wake geometries at various operating conditions are shown in Fig. 4 - Fig. 6. These wake geometries are the nondimensional cross sectional trajectories of the circular vortices of each rotor wake at three different axial spacings, D/R = 0.1, 0.2, 0.3, under the condition that each of them could produce the same total thrust. TAU and PL/PU in these figures represent τ and ν, the thrust and the power sharing ratio between rotors.

It should be noticed that each of these figures is corresponded with the typical wake geometries for $\nu < 1$, $\nu \doteqdot 1$, $\nu > 1$, respectively. From an analogy with the conclusions of the generalized momentum analysis, the performances and wake geometries depicted in Fig. 5 are understood to be those of near optimum condition whereas the other two cases are not under optimum conditions. It is clearly shown in these figures that the wake geometries of a co-axial rotor in hover are varied remarkably with the combinations of the thrust sharing ratios and the axial spacings and the most important cues to define the optimum performance can be detected by the behaviours of vortices in near wake region of the lower rotor. It is also interesting to note that in Fig. 5, as no axial velocity can be found near the outer part of the lower rotor disc, which is resulted from non-linear interactions between vortices, the behaviours of vortices in the lower rotor wake are characterized by more predominant radial movements rather than axial ones and the wake boundary of the lower rotor can be formulated in close vicinity of the contracted upper rotor wake. The thrust sharing ratio for this case become almost equal to the contraction ratio at the lower rotor.

Those unique features of the wake geometries which govern the optimum performance of a co-axial rotor in hover are well consistent with the conclusions deduced from the generalized momentum theory and the important role of the rotor-wake interference effect for the performance optimization of a co-axial rotor in hover is explored.

4. CONCLUSIONS

Basic researches for the performance optimization of a co-axial rotor in hover are carried out using the generalized momentum theory and the simplified free wake analysis. Dealing with a co-axial rotor as one of the variable geometry rotor, the effects of the axial spacings and the thrust sharing ratio between rotors on the hover performances are clarified and the optimum hover performance is established in relation to its wake geometries. It is clearly understood that the mutual interference effects of the contracted upper rotor wake on the outer part of the lower rotor disc could play a important role for the performance optimization of a co-axial rotor in hover. The inclusion of viscous diffusion effects of vortices will be anticipated for more rigorous and precise estimation of the hover performances and the wake geometries of a co-axial rotor.

REFERENCES

1. D. R. Clark, A. C. Leiper — The Free Wake Analysis, 25th Forum, A.H.S., No.321, 1969

2. W. Z. Stepniewski — Rotary-Wing Aerodynamics, Vol. I, NASA CR 3082, 1979

3. W. Johnson — Helicopter Theory (Book) Princeton University Press, 1980

4. V. E. Baskin, L. S. Vil'dgrube, Ye. S. Vozhdayev, G. I. Maykapav — Theory of the Lifting Airscrew, NASA TTF-823, 1976

5. A. J. Landgrabe, E. D. Bellinger — Experimental Investigation of Model Variable-Geometry and Ogee Tip Rotors, 29th Forum, A.H.S., No.703, 1973

6. M. J. Andrew — Co-Axial Rotor Aerodynamics in Hover, 6th European Rotorcraft and Powered Lift Aircraft Forum, No.27, 1980

7. T. Nagashima, H. Ouchi, F. Sasaki — Optimum Performance and Load Sharing of Co-Axial Rotor in Hover, Journal of Japan Society for Aeronautical and Space Sciences, Vol. 26, No.293, pp 325-333, 1978 (in Japanese)

8. T. Nagashima, K. Shinohara, T. Baba — A Flow Visualization Study for Tip Vortex Geometry of Co-Axial Rotor in Hover, Journal of Japan Society for Aeronautical and Space Sciences, Vol. 25, No.284, pp 442-445, 1977 (in Japanese)

9. H. Glauert — Aerodynamic Theory (Book), Vol. IV, Dover Publications, Inc., 1934

10. H. Lamb — Hydrodynamics (Book), 6th Edition, Cambridge University Press, 1932

11. J. D. Kocurek, L. F. Berkowitz, F. D. Harris — Hover Performance Methodology at Bell Helicopter Textron, 36th Forum, A.H.S., No.80-3, 1980

12. A. J. Landgrabe — An Analytical Method for Predicting Rotor Wake Geometry, Journal of The American Helicopter Society, Vol. 14, No.4, pp 20-32, 1969

13. A. R. S. Bramwell — On the Static Pressure in the Wake of A Hovering Rotor, Vertica, Vol. 1, pp 223-230, 1977

14. A. J. Landgrabe — An Analytical and Experimental Investigation of Helicopter Rotor Hover Performance and Wake Geometry Characteristics, USA AMRDL, Technical Report 71-24, 1971

15. J. L. Wu, R. K. Sigman — Optimum Performance and Potential Flow Field of Hovering Rotor, NASA CR 137705, May, 1975

16. M. C. Cheney, A. J. Landgrabe — Rotor Wakes - Key to Performance Prediction, AGARD CP-111, 1972

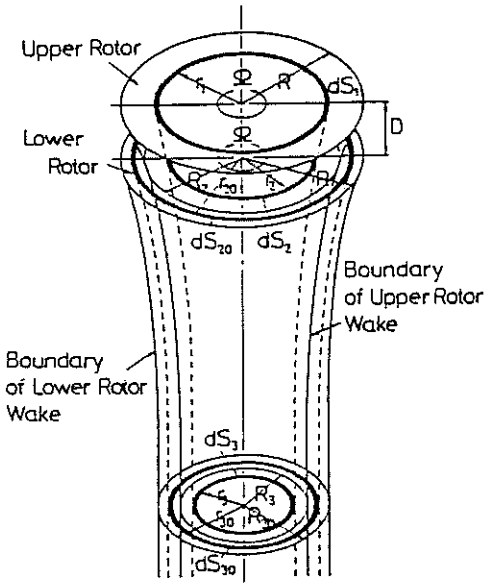

Fig.1 Wake Model of Co-Axial Rotor in Hover

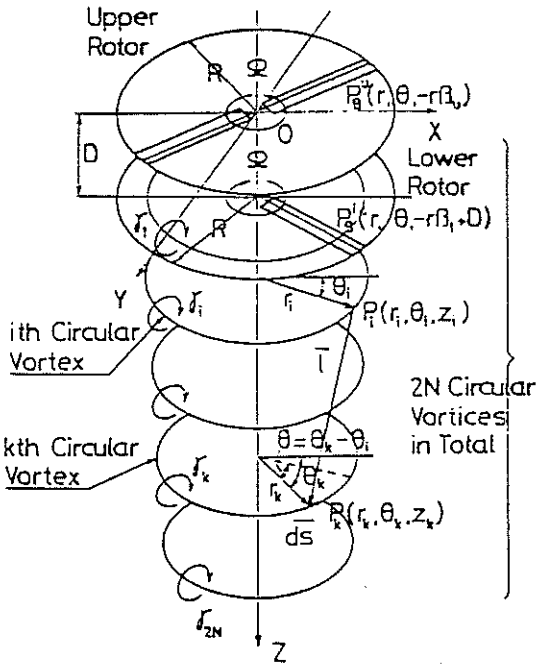

Fig.3 Discrete Circular Vortices Approximation for Wakes of Co-Axial Rotor in Hover

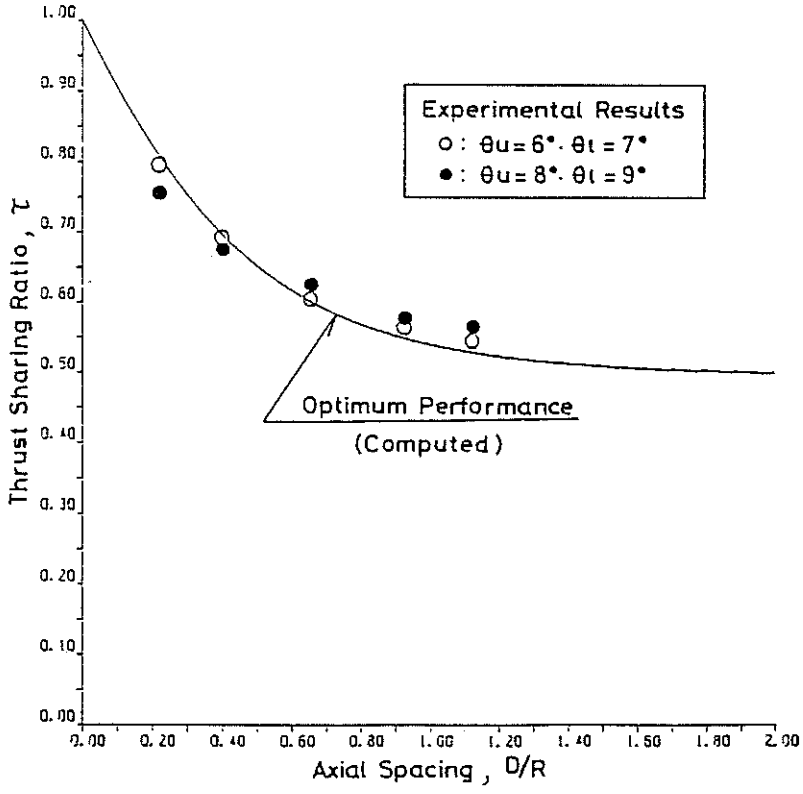

Fig.2 Effect of Axial Spacing on Optimum Performance and Comparision of Numerical Results with Experimental Ones.

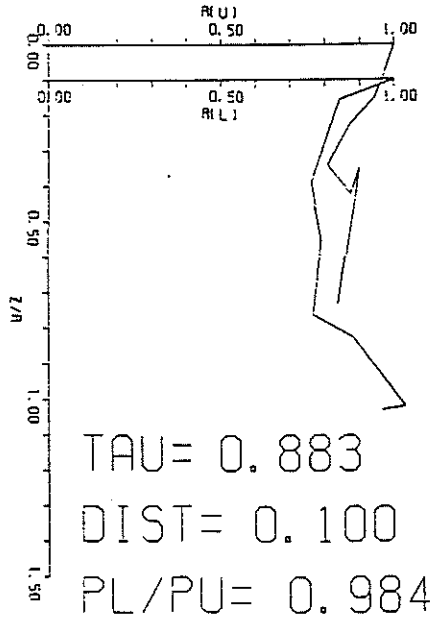

Fig.4 Wake Geometries of Co-Axial Rotor in Hover,D/R=0.1

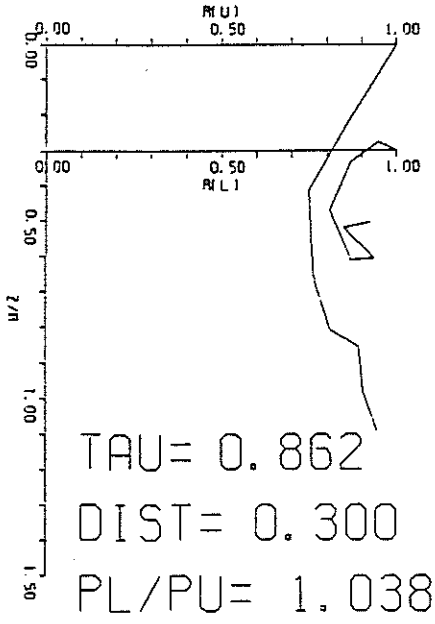

Fig.6 Wake Geometries of Co-Axial Rotor in Hover,D/R=0.3

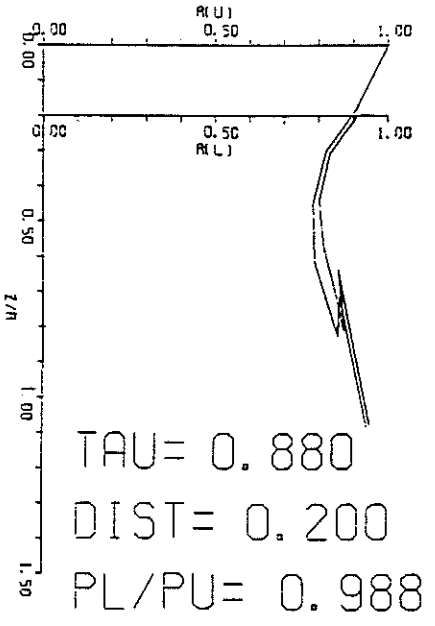

Fig.5 Wake Geometries of Co-Axial Rotor in Hover,D/R=0.2